Impacts of variations in Caspian Sea surface area on catchment-scale and large-scale climate

Koriche, S. A. ORCID: https://orcid.org/0000-0003-1285-2035, Nandini-Weiss, S. D., Prange, M., Singarayer, J. S., Arpe, K., Cloke, H. L., Schulz, M., Bakker, P., Leroy, S. A. G. and Coe, M. (2021) Impacts of variations in Caspian Sea surface area on catchment-scale and large-scale climate. Journal of Geophysical Research: Atmospheres, 126 (18). e2020JD034251. ISSN 2169-8996 doi: https://doi.org/10.1029/2020JD034251 Available at https://centaur.reading.ac.uk/100109/

JGR Atmospheres

RESEARCH ARTICLE
10.1029/2020JD034251

Impacts of Variations in Caspian Sea Surface Area on Catchment-Scale and Large-Scale Climate

Sifan A. Koriche[1,2,3,4], Sri D. Nandini-Weiss[5,6], Matthias Prange[5], Joy S. Singarayer[1], Klaus Arpe[7], Hannah L. Cloke[1,8,9,10], Michael Schulz[5], Pepijn Bakker[11], Suzanne A. G. Leroy[12,13], and Michael Coe[14]

[1]Department of Meteorology, University of Reading, Reading, UK, [2]School of Civil and Environmental Engineering, JiT, Jimma University, Jimma, Oromiyaa, [3]Department of Geoscience, Baylor University, Waco, TX, USA, [4]Jackson School of Geosciences, The University of Texas at Austin, Austin, TX, USA, [5]MARUM – Center for Marine Environmental Sciences, University of Bremen, Bremen, Germany, [6]Institute of Oceanography, Center for Earth System Research and Sustainability (CEN), University of Hamburg, Hamburg, Germany, [7]Max-Planck-Institute for Meteorology, Hamburg, Germany, [8]Department of Geography and Environmental Science, University of Reading, Reading, UK, [9]Department of Earth Sciences, Uppsala University, Uppsala, Sweden, [10]Centre of Natural Hazards and Disaster Science, CNDS, Uppsala, Sweden, [11]Department of Earth Sciences, Vrije Universiteit Amsterdam, Amsterdam, The Netherlands, [12]Aix Marseille University, CNRS, Aix-en-Provence, France, [13]School of Environmental Sciences, University of Liverpool, Liverpool, UK, [14]Woodwell Climate Research Centre, Falmouth, MA, USA

Abstract The Caspian Sea (CS) is the largest inland lake in the world. Large variations in sea level and surface area occurred in the past and are projected for the future. The potential impacts on regional and large-scale hydroclimate are not well understood. Here, we examine the impact of CS area on climate within its catchment and across the northern hemisphere, for the first time with a fully coupled climate model. The Community Earth System Model (CESM1.2.2) is used to simulate the climate of four scenarios: (a) larger than present CS area, (b) current area, (c) smaller than present area, and (d) no-CS scenario. The results reveal large changes in the regional atmospheric water budget. Evaporation (e) over the sea increases with increasing area, while precipitation (P) increases over the south-west CS with increasing area. P-E over the CS catchment decreases as CS surface area increases, indicating a dominant negative lake-evaporation feedback. A larger CS reduces summer surface air temperatures and increases winter temperatures. The impacts extend eastwards, where summer precipitation is enhanced over central Asia and the north-western Pacific experiences warming with reduced winter sea ice. Our results also indicate weakening of the 500-hPa troughs over the northern Pacific with larger CS area. We find a thermal response triggers a southward shift of the upper troposphere jet stream during summer. Our findings establish that changing CS area results in climate impacts of such scope that CS area variations should be incorporated into climate model simulations, including palaeo and future scenarios.

Plain Language Summary The Caspian Sea is the largest land-locked water body in the world. It is filled by rivers draining a vast region from northern Russia to Iran. The size of the Caspian Sea has varied considerably over recent centuries and millennia due to various factors, including changes in climate. Conversely, as the area of the sea changes it also has impacts on the climate, but there are significant questions about how and where those impacts would be felt. In this study we used a state-of-the-art climate model in which we specified different sizes of Caspian Sea in order to examine how the climate changes as its area increases. We observed that the local seasonal cycle of temperatures gets smaller, and evaporation increases, while there are more spatially complex changes in local rainfall. Furthermore, the impacts on atmospheric circulation occur as far as the north Pacific, with resulting increases in temperature and decreases in sea-ice coverage in winter as the Caspian area increases. The climate impacts are so significant and geographically extensive that climate models used to simulate climate change (both in future and past scenarios) should incorporate changes to the Caspian Sea area if they are to robustly model regional climate.

Sifan A. Koriche and Sri D. Nandini-Weiss contributed equally to this work and share joint first authorship.
Klaus Arpe is retired.

Key Points:

- Surface water budget over the Caspian catchment decreases as surface area increases due to negative lake surface-evaporation feedback
- A larger Caspian Sea enhances precipitation over central Asia, warms the north-western Pacific during winter, and reduces Pacific sea ice
- Accurate representation of the Caspian Sea in climate models is important to avoid creating additional biases both locally and globally

Supporting Information:

Supporting Information may be found in the online version of this article.

Correspondence to:

S. A. Koriche and S. D. Nandini-Weiss, s.koriche@reading.ac.uk; numarsanifa@gmail.com; snandini@marum.de

Citation:

Koriche, S. A., Nandini-Weiss, S. D., Prange, M., Singarayer, J. S., Arpe, K., Cloke, H. L., et al. (2021). Impacts of variations in Caspian Sea surface area on catchment-scale and large-scale climate. *Journal of Geophysical Research: Atmospheres*, *126*, e2020JD034251. https://doi.org/10.1029/2020JD034251

Received 13 NOV 2020
Accepted 8 SEP 2021

Author Contributions:

Conceptualization: Sifan A. Koriche, Sri D. Nandini-Weiss, Matthias Prange,

1. Introduction

The Caspian Sea (CS) is the world's largest inland sea, sited within a vast endorheic catchment area (3.6 Mkm^2) that is fed by 130 rivers (Rodionov, 1994). Currently, >80% of inflow contribution is from the

Joy S. Singarayer, Klaus Arpe, Hannah L. Cloke
Formal analysis: Sifan A. Koriche, Sri D. Nandini-Weiss
Funding acquisition: Matthias Prange, Joy S. Singarayer, Michael Schulz
Investigation: Sifan A. Koriche, Sri D. Nandini-Weiss
Methodology: Sifan A. Koriche, Sri D. Nandini-Weiss, Pepijn Bakker
Supervision: Matthias Prange, Joy S. Singarayer, Hannah L. Cloke, Michael Schulz
Visualization: Sifan A. Koriche, Sri D. Nandini-Weiss
Writing – original draft: Sifan A. Koriche, Sri D. Nandini-Weiss
Writing – review & editing: Sifan A. Koriche, Sri D. Nandini-Weiss, Matthias Prange, Joy S. Singarayer, Klaus Arpe, Hannah L. Cloke, Michael Schulz, Pepijn Bakker, Suzanne A. G. Leroy, Michael Coe

Volga and the CS water level is ∼28 m below global mean sea level (Leroy et al., 2020). The CS is situated amid semi-arid Central Asian regions, flat northern terrains, and humid high mountain ranges in Eurasia (Figure 1). A large region vulnerable to desertification lies west of the northern CS (Republic of Kalmykia), and a region of high precipitation (the Hyrcanian region) is found south of the CS (Molavi-Arabshahi et al., 2016). Given the complex orography and extensive geography, the entire CS catchment area occupies six Köppen climatic zones (Chen & Chen, 2013).

Over the Quaternary period, the CS experienced extreme water-level changes ranging from approximately +50 m to −90 m between transgressive and regressive periods, and variations of >3 m during the last century (Arpe & Leroy, 2007; Arslanov et al., 2016; Bezrodnykh et al., 2020; Forte & Cowgill, 2013; Kakroodi et al., 2014, 2015; Kislov et al., 2014; Krijgsman et al., 2019; Kroonenberg et al., 2008; Leroy et al., 2020; Naderi-Beni et al., 2013; Yanina et al., 2020; Yanina, 2014). Such large variations in water level have substantial impacts on the change in CS surface area (Figure 1). The difference in area between late Quaternary low stands and high stands is roughly equivalent to 70% of current CS area, and this difference can potentially affect regional and large-scale hydroclimate (Arpe & Leroy, 2007). Understanding the feedbacks of CS area variations on the hydroclimate system is essential at both the regional and global scale, since any large waterbody like the CS plays a significant role in affecting the energy and water budget by altering the albedo, evaporative fluxes, and near-surface temperature.

The influence of the presence of the CS on regional and large-scale climate can be inferred from previous climate modeling studies. Several have examined the impacts on the CS itself (Arpe et al., 2019; Lodh, 2015; Nicholls & Toumi, 2014) and some have examined other large lakes, e.g., mega-lake Chad (Broström et al., 1998; Coe & Bonan, 1997; Contoux et al., 2013) or the Great Lakes (Lofgren, 1997; Notaro et al., 2013; Sousounis & Fritsch, 1994). Idealized studies of the Great Lakes have noted that their presence impacts large-scale circulation patterns and the jet stream (Lofgren, 1997), with increased strength of zonal winds and enhanced cyclogenesis associated with anomalous heat and moisture transport Sousounis and Fritsch (1994). Another study on the effects of the Great Lakes on large-scale circulation found that the lakes caused decreased (increased) surface pressure in winter (summer), which led to irregular cyclonicity (anticyclonicity) over the lakes (Notaro et al., 2013). However, they found no shift in the jet stream, unlike other studies (e.g., Lofgren, 1997), likely due to constraints in the regional modeling domain.

Most climate models still poorly prescribe the actual CS area, in part due to their relatively low spatial resolutions. This may bias its climatic impacts and introduce errors in the CS water budget (Arpe et al., 2019; Nandini-Weiss et al., 2020). Previous studies have employed global or regional climate models to understand the influence of changing CS surface areas on regional and large-scale climate. Using a regional climate model, Tsuang et al. (2001) and Nicholls and Toumi (2014) examined the impacts of the presence of the current CS area (when compared to no-CS) on seasonal precipitation and atmospheric circulation patterns. Their findings suggest that the presence of the CS leads to significant changes in surface temperatures over the CS, which increase in winter and decrease in summer. In particular, decreases in summer temperature, due to higher air density, influence the atmosphere via changes to geopotential height extending to the top of the troposphere, and zonal winds, leading to a stronger summer jet stream over western Asia. However, these studies did not investigate how the size of the surface area of the CS may impact climate explicitly.

On the other hand, using a global climate model, Arpe et al. (2019) examined the impacts of different CS areas and found that changes in evaporation over the sea were linearly related to CS surface area. They also found an increase of precipitation with in the CS catchment area, partly compensating the impact of increased evaporation for the water budget of the CS. Interestingly, they found that variations in CS surface area had an impact on the large-scale atmospheric circulation as far as the northern Pacific. However, their results may be affected by low resolution (T63), which limits the actual representation of the CS area and the topography around the CS. In addition, prescribed sea surface temperatures were used for the global ocean, with the aim to focus more on the direct impact of the CS area, which may limit the large-scale response to CS area variation.

The above studies suggest that the CS may have regional and remote effects on climate. However, there remain open questions about the manner and magnitude of the climatic feedbacks from realistic variations in CS surface area. Here, we apply a new modeling approach, involving a global state-of-the-art climate

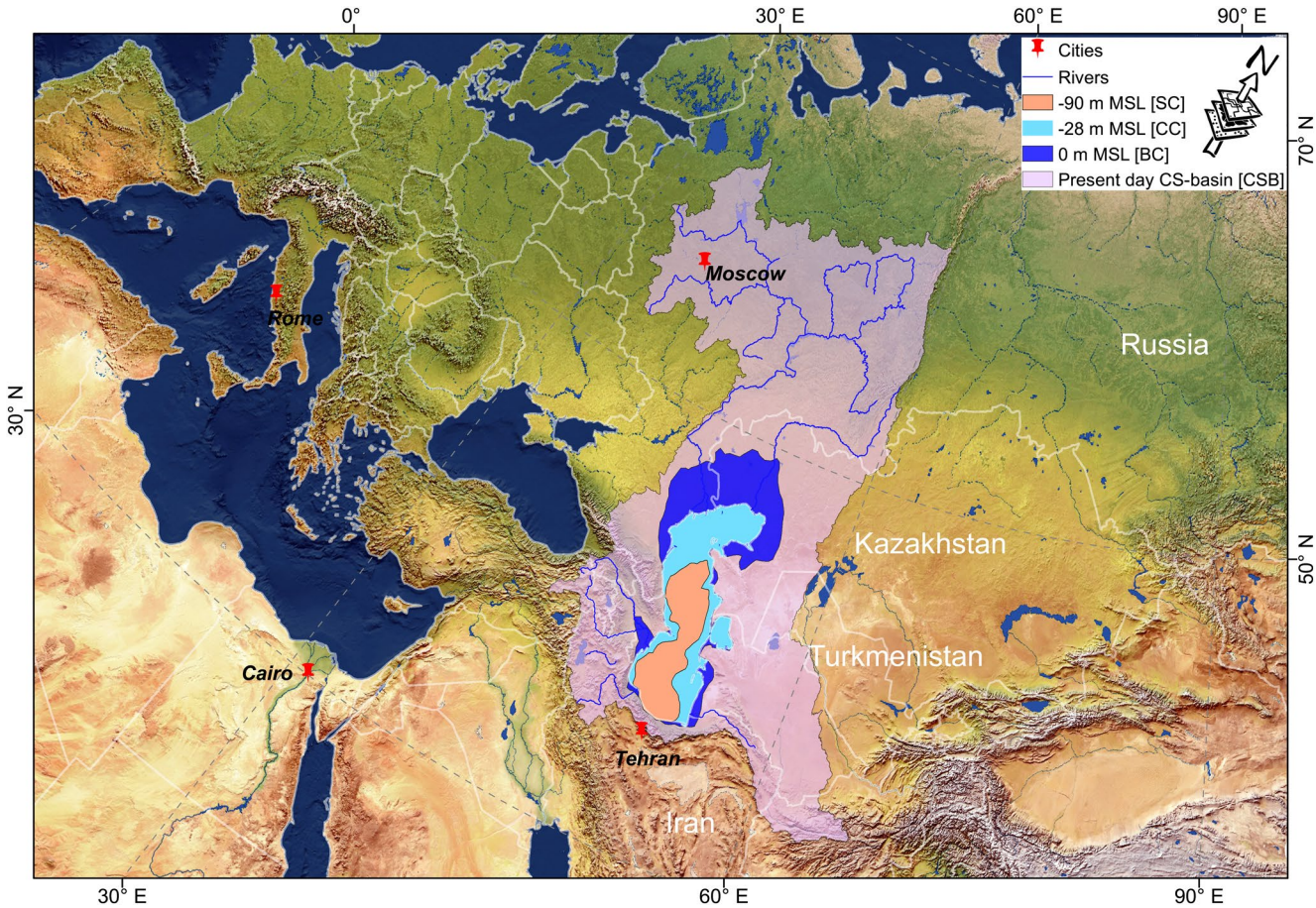

Figure 1. High-resolution Digital Elevation Model (DEM) contours of Caspian Sea surface areas (shown by dark blue area (large Caspian, BC), brown area (Small Caspian, SC) and light blue area (Current Caspian, CC). The catchment area is depicted by light purple area. Blue and white solid lines represent rivers and country borders respectively, and MSL refers to Mean Sea Level. Shaded relief, water, and drainages are made with Natural Earth (Free vector and raster map data @ https://www.naturalearthdata.com).

model and a hydrological routing model, to constrain the impacts from major surface area changes of the CS that are known to have occurred during the late Quaternary period. We use our modeling approach to investigate catchment-scale and large-scale effects of varying CS surface areas on hydroclimate, lake level and atmospheric circulation.

2. Methodology and Data

In this section, we describe the modeling methodology used and the data analysis performed. First, we designed four scenarios of different CS size (large, small, current and no Caspian) used to drive the Earth-system model CESM1.2.2 (Hurrell et al., 2013) to simulate the climate response. The large and small Caspian Sea scenarios are chosen to represent two cases of extreme Caspian Sea area change that occurred during the paleao period, and the current Caspian Sea scenario is selected to evaluate the effect of having a "realistic" Caspian Sea extent that represent present day area. Though the Caspian Sea has never fully desiccated since its formation, the no-Caspian Sea scenario is chosen as one of the scenario (and used as a reference) to evaluate the effect of including a Caspian Sea in a model as numerous climate models either not properly prescribe or ignore Caspian Sea (Koriche et al., 2021).

Second, we examined the regional catchment anomalies of water budget (precipitation - evaporation; P-E), surface air temperature and vertically integrated lower level (>850 hPa) water-vapor flux of large, current and small Caspian scenarios with respect to no-CS. The water-vapor flux was inferred from vertically integrated water-vapor transport calculated by integrating the zonal and meridional moisture fluxes via each

Table 1
CESM Model Components and Compset Used in This Study

Compset
•Name: B_1850_CAM5_CN (Pre-industrial)
•Boundary condition: pre-industrial
•Physics: cam5 and clm4.0
•NB: clm4.0 with carbon nitrogen cycle, prognostic CICE and POP2 default

Note. We used a component set configured for pre-industrial boundary conditions, which reflects land use/cover conditions consistent with 1850., except for the CS area changes introduced for this experiment.

atmospheric layer between 1,000 hPa and 850 hPa (seven model layers). This variable is used as a measure of the horizontal transport of atmospheric moisture (Sousa et al., 2020). Third, we repeated this for large-scale changes (sub-tropical jet stream, geopotential height and sea level pressure). Finally, we performed stand-alone numerical simulations of CS Level (CSL) using the Hydrological Routing Algorithm model (THMB; Coe, 1998, 2000) with climate forcing from the four scenarios in order to assess the feedback between CS surface area change and its water budget. Statistical analyses on all four simulations include annual mean and seasonal plots of winter (December, January, February-DJF), spring (March, April, May-MAM), summer (June, July, August-JJA) and autumn (September, October, November-SON). The statistical significance of seasonal and annual mean differences was estimated using a two–tailed Student t-test with 95% confidence level.

2.1. CESM1.2.2 Model Experimental Design

CESM is a fully coupled global climate model composed of five separate models simulating the Earth's atmosphere (Community Atmosphere Model, CAM5), ocean (Parallel Ocean Program, POP2), land (Community Land Model, CLM4.0), rivers (River Transport Model, RTM) and sea-ice (Community Sea Ice Model, CICE), plus one central coupler component (Hurrell et al., 2013). In this model version, the CS is set up to be part of the ocean model component as a marginal sea. The atmosphere and land components are set to 0.9° latitude by 1.25° longitude horizontal resolution. The atmosphere component has 30 vertical levels, whereas, the ocean component has 60 vertical levels. Both ocean and sea ice components use a horizontal grid mesh of 384 by 320 cells.

Evaluation of the model version used in this study (1° version of CESM1.2.2, Table 1) and a 2° version model with two different atmospheric physics components (CAM4 and CAM5), has been carried out previously in Nandini-Weiss et al. (2020). According to their results, the higher resolution model with the improvements to atmospheric physics performance was considerably better over the Caspian Sea region than the other versions, when considering surface air temperature, precipitation, and evaporation, as well as NAO teleconnections. Orography-based biases were also smallest in this version, and over all the 1 CAM5 model was deemed to have a sufficient level of skill in modeling climate in the region of the sea.

Four numerical sensitivity experiments were carried out at the North German Supercomputer HLRN3. Each simulation had pre-industrial (1850s) climate boundary conditions as this is a standard baseline reference for most climate modeling runs. At the pre-industrial the levels of atmospheric greenhouse gases are assumed to be minimally altered by anthropogenic emissions, enabling the pre-industrial scenario to be compared to future anthropogenic or palaeo simulations, or other changes to boundary conditions. The four simulations only differ in the CS prescribed areas. Readers are advised to refer to the supplementary file, Figure S1, showing the representations of CS size for each scenario in the ocean and land components of the CESM1.2.2 model.

2.2. CESM Caspian Sea Areas and Input Data Preparation

The three CS surface areas (large, current and small; Figure 1) correspond to lake levels of 0, −28 and −90 m above mean sea level, respectively, and were determined using a 1 arc minute ETOPO1 Digital Elevation Model (DEM) (Amante & Eakins, 2009) and spatial analysis tools in ArcGIS 10.5.1. The resultant CS areas

were overlain onto the CESM default ocean domain file in order to identify and modify the land and ocean grid points. If the water level of a grid point (ocean grid cells) was lower than the mean bathymetry of the grid, the grid cell is set to be land. The large Caspian simulation is actually the default CESM pre-industrial simulation, which includes a CS surface area that is larger than the present-day area.

Based on the new CS areas, the CESM ocean bathymetry was modified for the changes made to land/ocean areas. Next, new surface-flux mapping files were generated with the NCAR Paleo toolkit software to prepare all input files, which were interpolated onto the same domain. For all four scenarios, we extrapolated the surface properties of the nearest neighbor grid cell to the new land grid cells (e.g., plant functional types and soil properties). The land properties were recalculated for each scenario. The CESM simulations were spun up for 100 years (initialized from a standard pre-industrial control state) and the last 50 years were taken for analysis in our sensitivity study. In this study, we examined differences between all simulations with respect to a no-CS scenario.

2.3. The Hydrological Model: THMB

The hydrological model THMB (which was formerly called HYDRA, Hydrological Routing Algorithm; Coe, 1998) was used to simulate the level of the CS based on the outputs from the CESM climate simulations with the aim to validate the P-E that the climate model produced over the Caspian Sea drainage area. For detailed information about THMB, readers are advised to refer to Coe (1998, 2000). Four offline simulations of the CS level were performed using input boundary conditions derived from the large, current, small, and no-CS climate simulations. The mean monthly climatology averaged over the last 50 years of the climate simulations was used to drive the THMB simulations. The THMB model simulations were spun up for 1,000 years. The forcing that the THMB model simulations are based on is the long term monthly climatology (50 year mean) in an iterative way.

THMB simulates hydrological processes as a linked dynamic system in which locally derived runoff is transported across the land surface in rivers, lakes and wetlands, and is finally transported to the ocean or an inland lake (Coe, 1998, 2000). The model is forced with estimates of runoff over land, and precipitation and evaporation over sea, in a hydrologic network linked to a linear reservoir model (Equation 1). The linear reservoir model (river water reservoir (Wr), surface runoff pool (Ws), and subsurface drainage pool (Wd)) simulates water transport based on prescribed local drainage directions derived from the local topography, residence times of water within a grid cell, and effective flow velocities, given in Equation 1:

$$\partial\left[W_r\right]/\partial t = \left[W_s/T_s + W_d/T_d\right] * \left[1 - A_w\right] + \left[P_w - E_w\right] * A_w - \left[W_r/T_r\right] + \sum F_{in} \quad (1)$$

where A_w is the predicted fractional water area in the grid cell; T_s, T_d, and T_r are the residence times (s) of the water in each of the reservoirs; P_w and E_w are the precipitation and evaporation rates (m^3s^{-1}) over the surface water, respectively; and F_{in} is the water flux from the upstream cells (m^3s^{-1}). For the case of small and no-CS scenarios, where considerable areas were changed to land, we estimated potential evaporation for E_w (over water) in Equation 1 rather than actual evaporation from the climate model in order to simulate CSL with THMB. This approach assumes that actual and potential evaporation over a water body are effectively equal, and it was chosen in order to account for the increases in evaporation that would be expected if the CS area increases during the simulation. If this is not accounted for then the volume of water in the small-CS and no-CS scenarios would keep increasing until overflowing into the neighboring drainage basin (Black Sea, the sill height is 40 m above sea level) because the prescribed evaporation rate from the CS is too small (as it would be taken from land grid cells). Potential evaporation provides a more realistic estimate of E_w over areas that convert from land to water during the course of the THMB simulation. Estimates of evaporation over water surface are those used by Coe (1998) and are calculated using the simplified Penman (without recourse to wind data) formulation relating equilibrium evaporation from a wet surface to the net surface radiation using monthly average estimates of climate fields from CESM for small and no-CS experiments (Coe, 1998; Peixoto & Oort, 1992; Valiantzas, 2006). From the climate model fields, monthly average estimates of surface temperature and cloud cover (used to estimate potential sunshine) are linearly interpolated to quasi-daily values and used to derive the net surface radiation. The daily equilibrium evaporation values are then summed to provide monthly mean values as the other climate fields (precipitation over sea

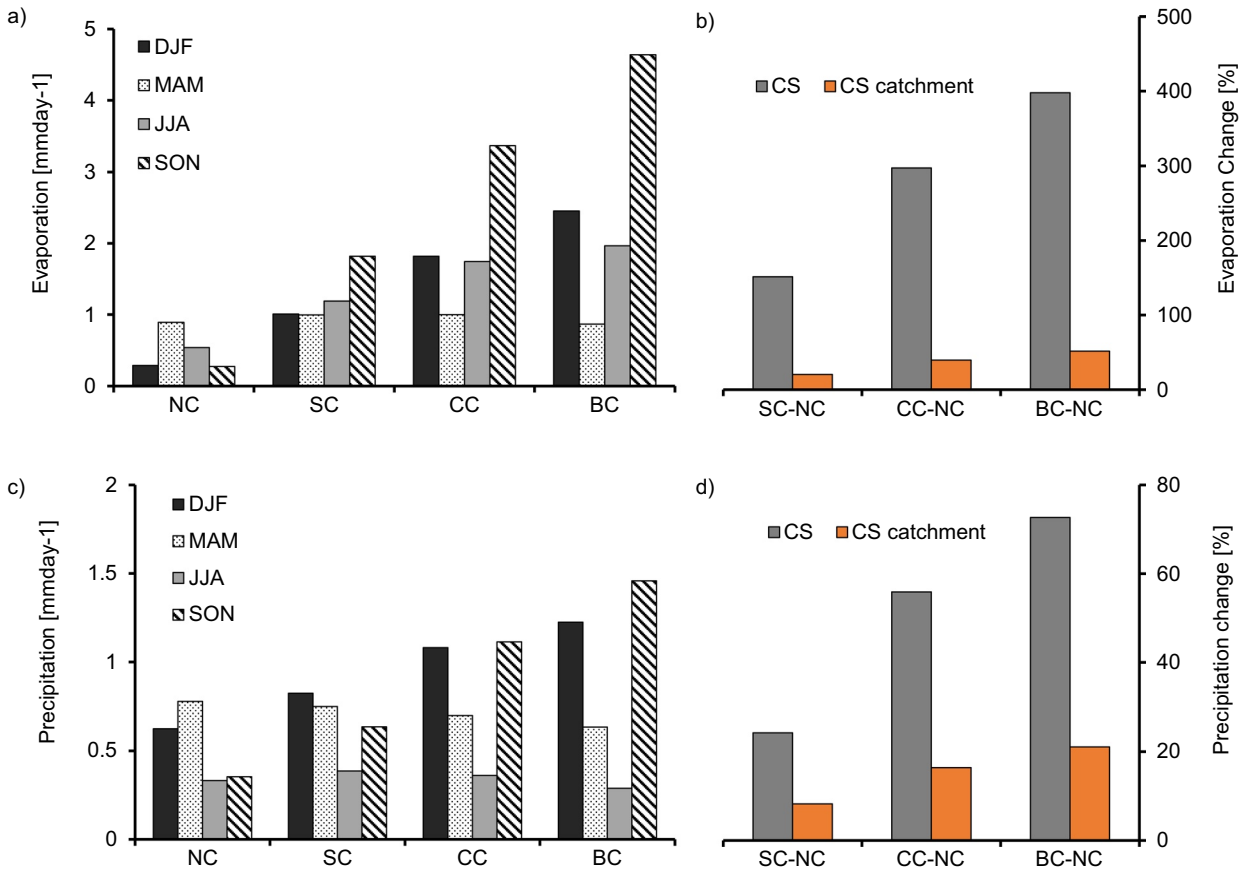

Figure 2. (a) Mean seasonal evaporation over CS surface area, (b) mean annual percentage change of evaporation relative to no-CS scenario over CS surface area (in gray) and CS catchment (in orange), (c) same as 'a' but for precipitation, and (d) same as 'b' but for precipitation. Area of interest considered for calculation: large Caspian Sea (referred in the figure as 'CS') and CS drainage basin including land and water surfaces (referred in the figure as 'CS catchment') (Key: BC–Large CS, CC–Present-day CS, SC–small CS, NC–No-CS, DJF–December/January/February, MAM–March/April/May, JJA–June/July/August, SON–September/October/November).

and runoff) used in THMB are on monthly time steps. According to Coe (1998), a realistic estimation of open water evaporation using the Penman method has been achieved. Comparison of CESM and Penman based evaporation estimate for Caspian Sea shows comparable result (Figure S2). The mean annual evaporation rates over Caspian Sea simulated by Penman method is generally within 10%–12% of evaporation rates from CESM.

3. Results

3.1. The Impact of CS Surface Area on Regional Climate

Here we present the impacts of varying CS area on surface water budget (evaporation and precipitation), CSL, lower level vertically integrated water-vapor transport (IVT), and 2-m air temperature (T2m). All results presented below are based on monthly climatological model output.

Our findings show that the variation of CS area has a strong influence on the regional climate. Across the four scenarios evaporation increases as the CS surface area increases (Figure 2a). The mean annual evaporation increases up to ~400% over CS and ~50% over the CS catchment (over land and lake surface) for the BC scenario compared to no-CS (Figure 2b). Increases in evaporation across the CS catchment area directly follow from the increase in surface area of the CS itself. The annual mean evaporation anomaly over the wider CS catchment area is predominantly higher when a CS is present than with the no-CS scenario (more than 3 mmday^{-1} in places) (Figures 3a, 3e, and 3i). Higher evaporation over the CS is more pronounced

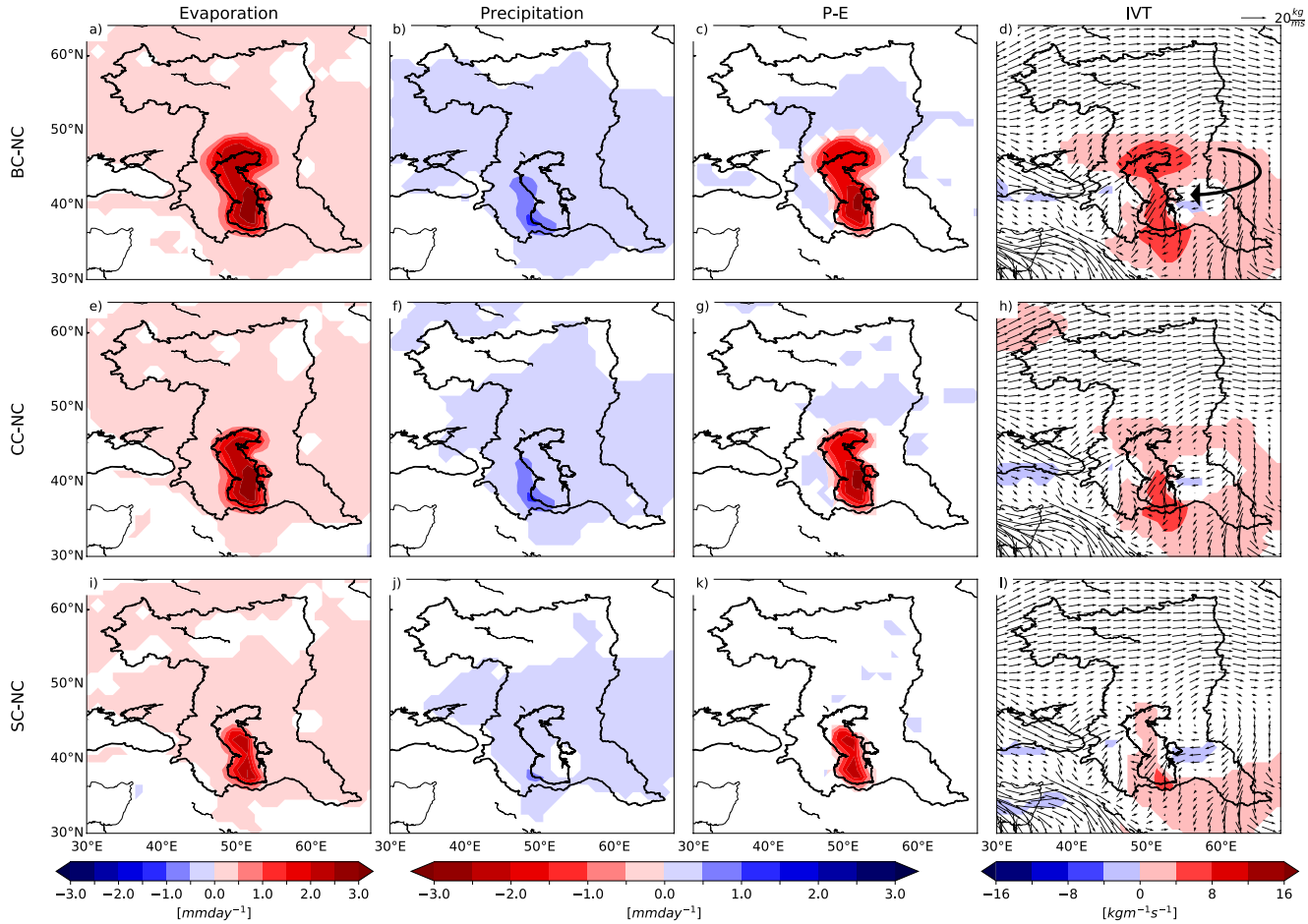

Figure 3. Annual mean changes for evaporation (a, e and i), precipitation (b, f and j), P-E (c, g and k) and lower level (1,000–850 hPa) vertically integrated water vapor transport (IVT) (d, h and l) for large, current and small CS with respect to No-CS scenario. The shaded colors are areas where mean anomaly is different from zero at 95% confidence level. The IVT is calculated by integrating the zonal and meridional moisture fluxes. The vector field are not anomaly values, but actual values of IVT for BC (d), CC (h) and SC (l).

during the autumn and winter seasons (Figure S3). This is because of greater thermal inertia resulting from higher heat capacity plus lower albedo of the lake compared to bare land surface. More heat (energy) is stored during spring and summer, which is released later during autumn and winter, leading to a warmer surface, lower atmospheric stability, and higher evaporation.

The changes in CS surface area contribute considerably to precipitation distribution and intensity (Figures 2c, 2d, 3b, 3f, 3j, and S4). The mean annual precipitation increases with a larger CS area by up to ~70% over the CS and ~20% over the CS catchment (over land and lake surface) for BC compared to no-CS scenario (Figure 2d). The largest precipitation anomalies (greater than 1 mmday^{-1}) occur over the south-western part of CS. The two possible primary reasons for higher precipitation in the south-western part of CS are the amount of evaporation available over the sea (which depends on the size of the sea and the length of air flow over sea to pick up moisture, i.e., fetch) and lower level easterly winds driving vapor flux in south-western direction (Figures 3d, 3h and 3l) toward the Caucasus and Elburz mountains (Arpe et al., 2019). Significant, though smaller, changes in the annual mean precipitation (<0.5 mmday^{-1}) are observed over most parts of the CS catchment area, which can be linked to the combined effect of lower level easterly wind driving the moisture flux and larger scale circulation processes. Seasonal changes of precipitation have a similar spatial pattern to changes in evaporation during autumn and winter (Figure S4), partly compensating for the water loss from the CS due to evaporation. The presence of a CS produces more precipitation over the sea in autumn and winter (more than 2 mmday^{-1}), but less precipitation over sea in spring and summer when surface cooling tends to stabilize the atmosphere (Figures 2c and S4). This indicates that winter and autumn

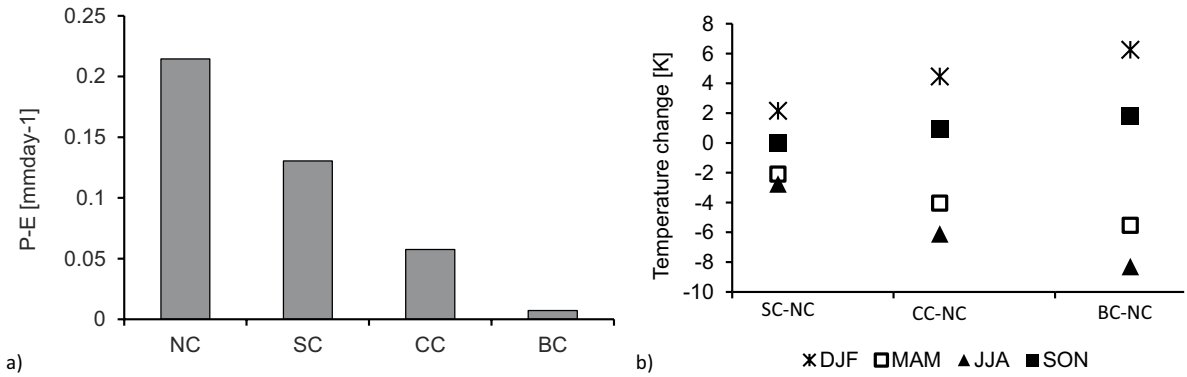

Figure 4. (a) Mean P-E over CS catchment, and (b) mean seasonal 2-m temperature (T2m) changes with respect to the no Caspian scenario over CS surface areas. Area of interest considered for calculation: drainage basin including land and water surfaces (for 'a') and large Caspian Sea (for 'b'). Abbreviations as in Figure 2.

precipitation changes dominate the annual mean anomalies. Although changes in precipitation tend to follow evaporation during autumn and winter, the changes are not linearly related throughout the year.

The enhanced evaporation over the CS in autumn leads to increased moisture in the atmosphere. This not only increases the precipitation over the CS itself but also the land around the CS. This has a consequence for evaporation in these areas. Arpe et al. (2020) hypothesized that with strong westerlies the enhanced moisture in the atmosphere might be blown to the east and lost from the water budget of the CS leading to a drop of the CSL and increase in the water levels of central Asian lakes.

The magnitude of the surface water budget (P-E) varies with CS surface area, both over the sea itself and the wider catchment (over land). P-E anomalies are negative over the CS since the evaporation increase greatly exceeds the precipitation increase over the sea surface (Figures 3c, 3g, 3k, and S5). P-E anomalies are positive over the land surface, where precipitation anomalies exceed the evaporation anomalies. These changes (greater than 3 $mmday^{-1}$ over CS) are more pronounced during autumn and winter seasons when the precipitation and evaporation changes are greater (Figure S5). The mean P-E over the CS catchment (land and lake surface) decreases as CS surface area increases, which indicates negative lake surface-evaporation feedback domination (Figure 4a). Changes in P-E would have direct impacts on CSL. As a closed drainage basin, variation of CS surface area strongly influences CSL change, as the amount of evaporation is positively related to changes in sea surface area. Based on offline CSL simulations with THMB using input boundary conditions from CS climate scenarios, the simulated CSLs were ~27.5 and ~25.25 m below mean sea level for current and large CS scenarios respectively. Prescribing the correct current CS area in CESM produces a CSL that is closer to the mean present-day observed sea level. The default representation of the CS in CESM (BC scenario) produced a CSL of ~2 m above the current observed state. The simulated CSL for small and no-CS scenarios were ~75 and ~138 m below mean sea level.

To understand the drivers of moisture transport that contribute to changes in water balance we investigate lower level IVT (>850 hPa). The vector fields represent the actual amount of IVT, whereas the color plot are the anomalies of IVT values with respect to no-CS (Figures 3d, 3h, and 3l). The moisture flux increases with larger CS area. Lower level wind patterns over the CS and the eastern part of the CS catchment form an anti-cyclonic pattern and this plays vital role in transporting moisture generated over the CS, as well as from the eastern part of the catchment area (Figure 3d). The easterly surface winds (from Kazakhstan and Turkmenistan) shift direction to the south-west around the western CS catchment area and this contributes significantly to the moisture flux directed toward the south-western parts of CS. The effect of westerly winds on the north CS is enhanced with larger CS area, as more water is available for evaporation in the north CS.

Changes in CS area also play a significant role in air temperature change over the CS and surrounding region. The results reveal strong responses in the regional annual mean T2m, where temperature significantly decreases (more than 3°C) over CS. Larger CS areas induce increases (decreases) in T2m during autumn and winter (spring and summer) seasons (Figures 4b and S6) Seasonal variation of T2m for larger CS clearly show significant decrease over and around the CS, predominately during spring and summer time

(Figures S6b, S6c, S6f, S6g, S6j, and S6k), when the amount of solar radiation received during this time is higher compared to other seasons. Coincidentally, the summer sea surface temperatures over the southern CS basin drop from 23.37°C (SC) to 21.21°C (CC) to 20.96°C (BC). This is as previously found by Arpe et al. (2019), who indicate that the expansion of the shallow northern part of the lake enhances evaporation, which leads to an enhanced loss of energy within the CS. This then causes a decrease of the SST in summer for the CS as a whole.

3.2. The Impact of CS Area Variation on Large Scale Climate

The results of this study show that the presence of different CS areas affect large-scale climate over the entire northern hemisphere. Annual changes show significant warming (>1°C) in surface air temperatures extending in a north easterly band over the northern catchment area and as far as east Siberia and north-west Pacific (Figures 5a–5c). The warming over the north-west Pacific increases from the small to large CS scenarios when compared with the no-CS scenario (Figures 5a–5c). Also, it appears that temperature changes are restricted in southern CS by the Elburz Mountains, which was also noted by Nicholls and Toumi (2014) and Arpe et al. (2019). The surface temperature anomaly patterns appear more spatially extensive when compared to precipitation where annual mean changes appear more focused on the regional surroundings of the CS catchment area (Figures 5d–5f). Upon examining the large-scale changes in sea level pressure as CS area increases, higher pressures are seen extending from the Mediterranean toward southern CS (anomalies of up to 125 Pa) (Figures 5g–5i).

The zonal winds at 200 hPa show changes in the jet stream, which plays a key role in distributing moisture, heat, and pressure across this region (Figures 5j–5l). The results indicate a north-south dipole anomaly in the jet stream pattern with a decrease in speed over the northern and central CS catchment area which extends in an easterly band across Asia and the north-west Pacific and decreases as CS area increases. The jet speed increases as CS area increases over the southern CS catchment area. In order to understand the influence of different CS areas on the mid tropospheric flow, we investigated changes in geopotential height and temperature at 500 hPa (Figure 6). Results show that annual mean temperatures (at 500 hPa) are associated with corresponding changes in geopotential height resulting in a weakening of the 500 hPa troughs over the northern Pacific as CS area increases (Figures 6d–6f). There is a significant link between decreases in temperature at 500 hPa and the reduction in geopotential height over the southern CS catchment area.

The seasonal results provide further insight into the processes by which different CS sizes influence large-scale climate over the entire northern hemisphere. Here, we only consider winter and summer changes and take the current CS scenario (compared to no-CS) as an example. For examining the seasonal changes for other CS sizes, the reader is directed to the supplementary figures (Figures S7 and S8), and these can be compared to the mean climatologies presented in Figures S9 and S10. The most striking and significant seasonal feature is the intense warming during winter for air temperatures over the CS and the northern catchment area, which extends as far afield as the north-west Pacific (Figure 7a). By comparison, the summer reduction in temperatures is restricted to the CS catchment area (Figure 7b). The mean winter temperature over the north-west Pacific region [51°N–72°N and 155°E–187.5°E] is calculated for all CS scenarios (Figure 7c). Generally, the warming increases from no-CS to large CS area. On the other hand, the winter increase in precipitation is mostly restricted to the CS region (Figure 7d; compare to Figure S9 for the mean climatologies). However, the summer increases over central Asia are of interest (>0.6 mm/day). Arpe et al. (2020) discuss the possibility of enhanced evaporation to transport moisture to the central Asian lakes where it is enhancing the precipitation; a process suggested here also (Figure 7e). When examined over the central Asia region [39°N–50.5°N and 62.5°E–100°E], precipitation tends to broadly increase for all simulations compared to the no-CS scenario (Figure 7f). This increase in summer precipitation over central Asia may be driven by the associated changes seen previously in surface winds, moisture flux, and the lake effects of the CS which transports moisture afield. However, this merits further investigation.

The winter sea level pressure anomalies show an east-west dipole over the CS catchment area and low pressure anomalies over the north-west Pacific (and Siberia), and high-pressure anomalies over Europe (and northeast Pacific) (Figure 8a). However, during summer high-pressure anomalies are seen over the CS, southern catchment area, and central Asia region (anomalies of up to 160 Pa) (Figure 8b).

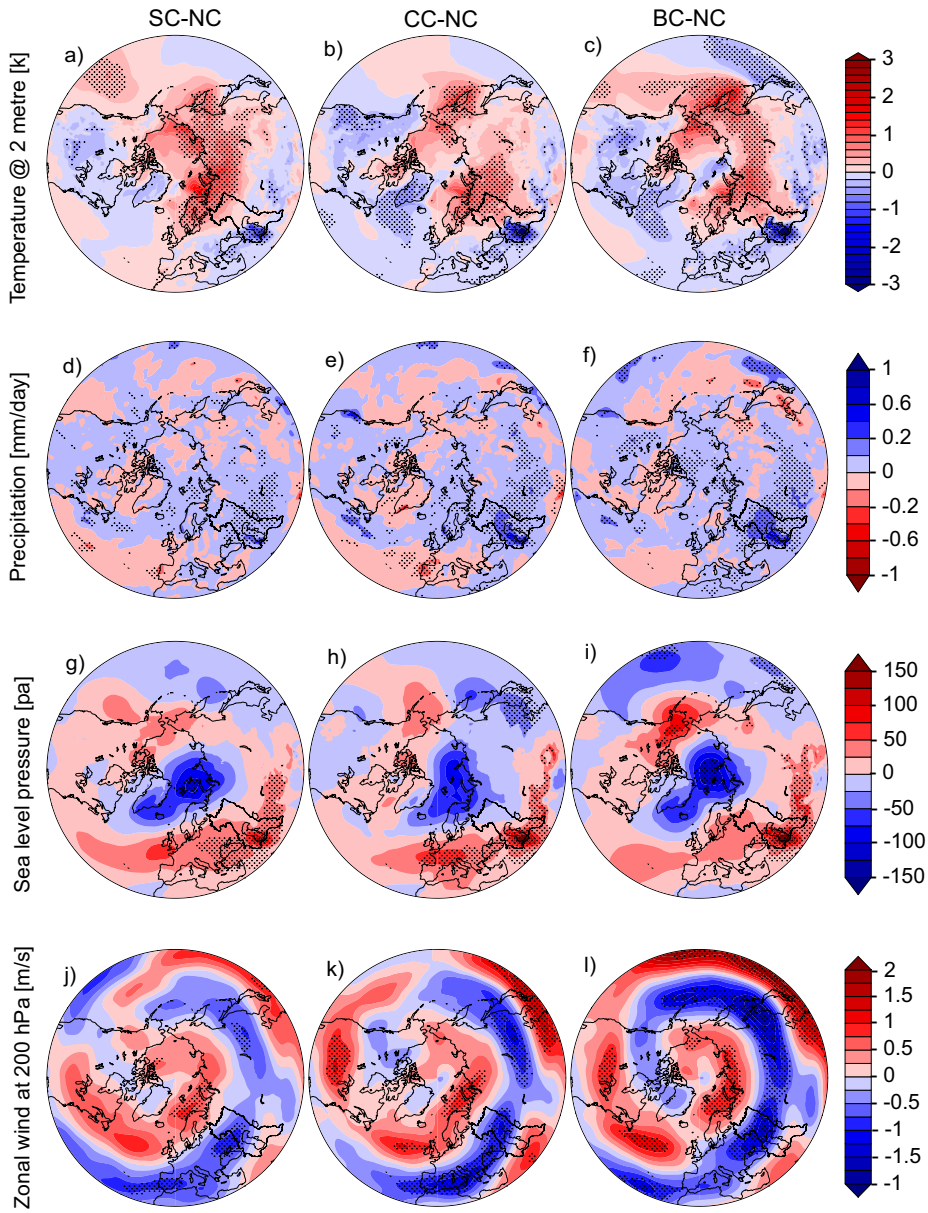

Figure 5. Annual mean changes of 2-m temperature (a, b and c), precipitation (d, e and f), sea level pressure (g, h and i) and zonal wind (j, k and l) at 200 hPa showing changes in the jet stream for small Caspian (SC), current Caspian (CC) and big Caspian (BC) with respect to no-Caspian (NC). Stippling indicates regions where the change is statistically significant at the 95% level based on a Student's t-test.

The presence of different CS sizes affects the mid (500 hPa) and upper (200 hPa) tropospheric circulation patterns. We first examined winter and summer changes for the geopotential height and the location of the jet stream by investigating the zonal winds at 200 hPa (Figures 8c–8f; compare to Figure S10 for the mean climatologies). The seasonal responses of both to the presence of different CS areas during winter and summer illustrate high seasonal differences, especially in the structure of the subtropical jet stream (Figures 8e and 8f). Reduced summer surface temperatures (Figure 7b) trigger a reduction in the summer geopotential height (~28 m) (Figure 8d) and a large-scale southward shift of the jet stream (Figure 8f) that was also observed in the annual mean anomalies. A possible explanation for this shift in the jet stream (also seen in Nicholls and Toumi (2014) arises from changing horizontal temperature gradients between warm and cold regions that influence the westerlies. Signals from surface temperature may propagate up to higher

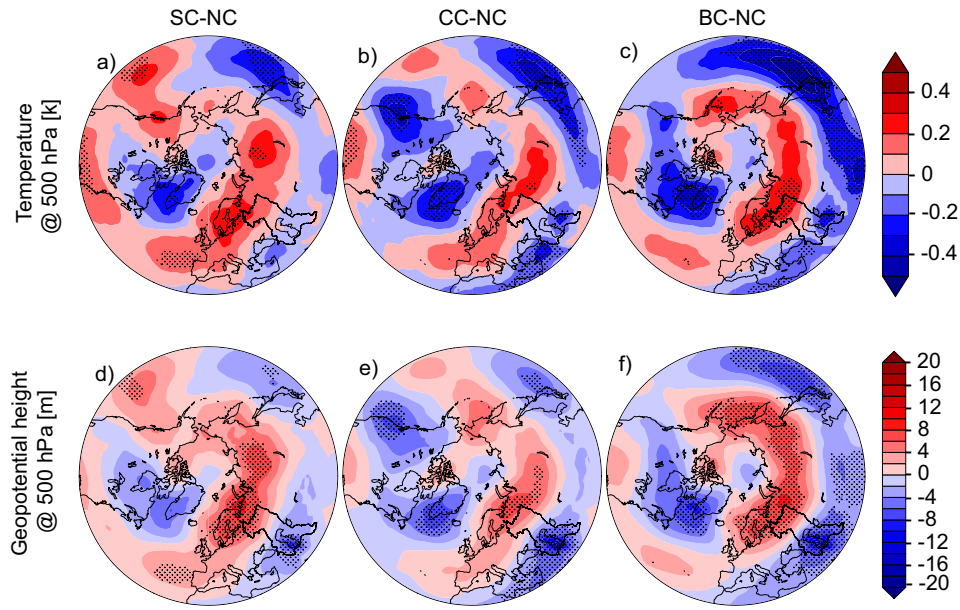

Figure 6. Same as Figure 5 but for temperature (a, b, and c) and geopotential height (d, e, and f) at 500 hPa.

atmospheric levels, affecting the geopotential height. The above summer relationship is consistent at the 500 hPa level as well (Figures 8g–8l).

Finally, we find that teleconnections in the large-scale atmospheric circulation significantly influence sea-ice conditions in the remote North Pacific and Arctic. As CS area increases, there is a reduction in sea-ice

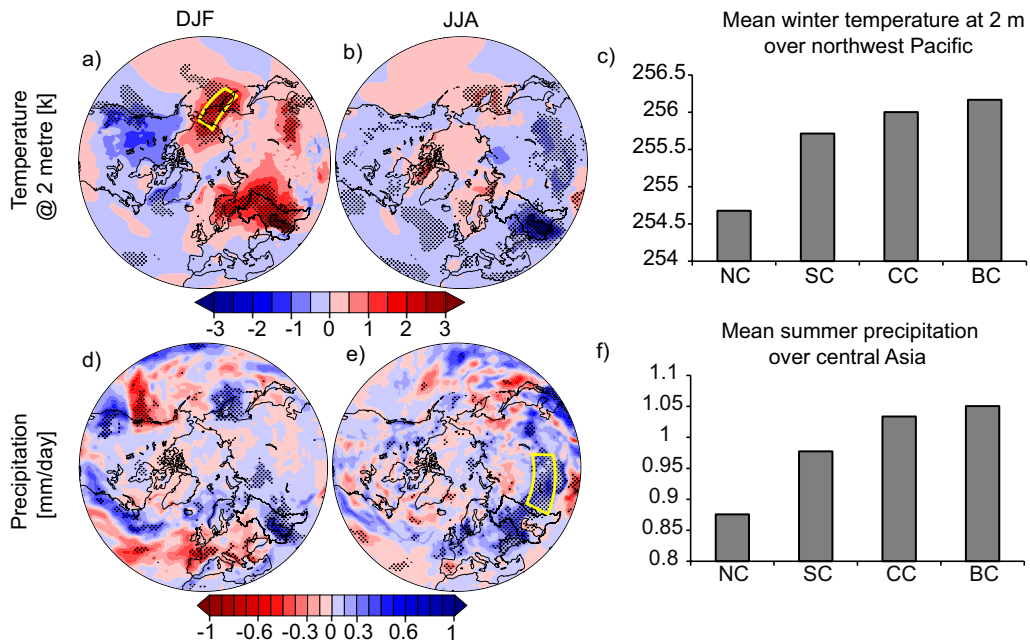

Figure 7. Winter and summer changes of 2-m air temperature (a and b respectively) and precipitation (d and e respectively) for current CS minus no-CS scenario. Mean winter 2-m temperature (c) averaged over north-west Pacific region [51°N–72°N and 155°E–187.5°E] (yellow box area), and mean summer precipitation (f) averaged over central Asia region [39°N–50.5°N and 62.5°E–100°E] (yellow box area) for the four CS surface area change scenarios. Stippling indicates regions where the change is statistically significant at the 95% level based on a Student's t-test. Abbreviations as in Figure 2.

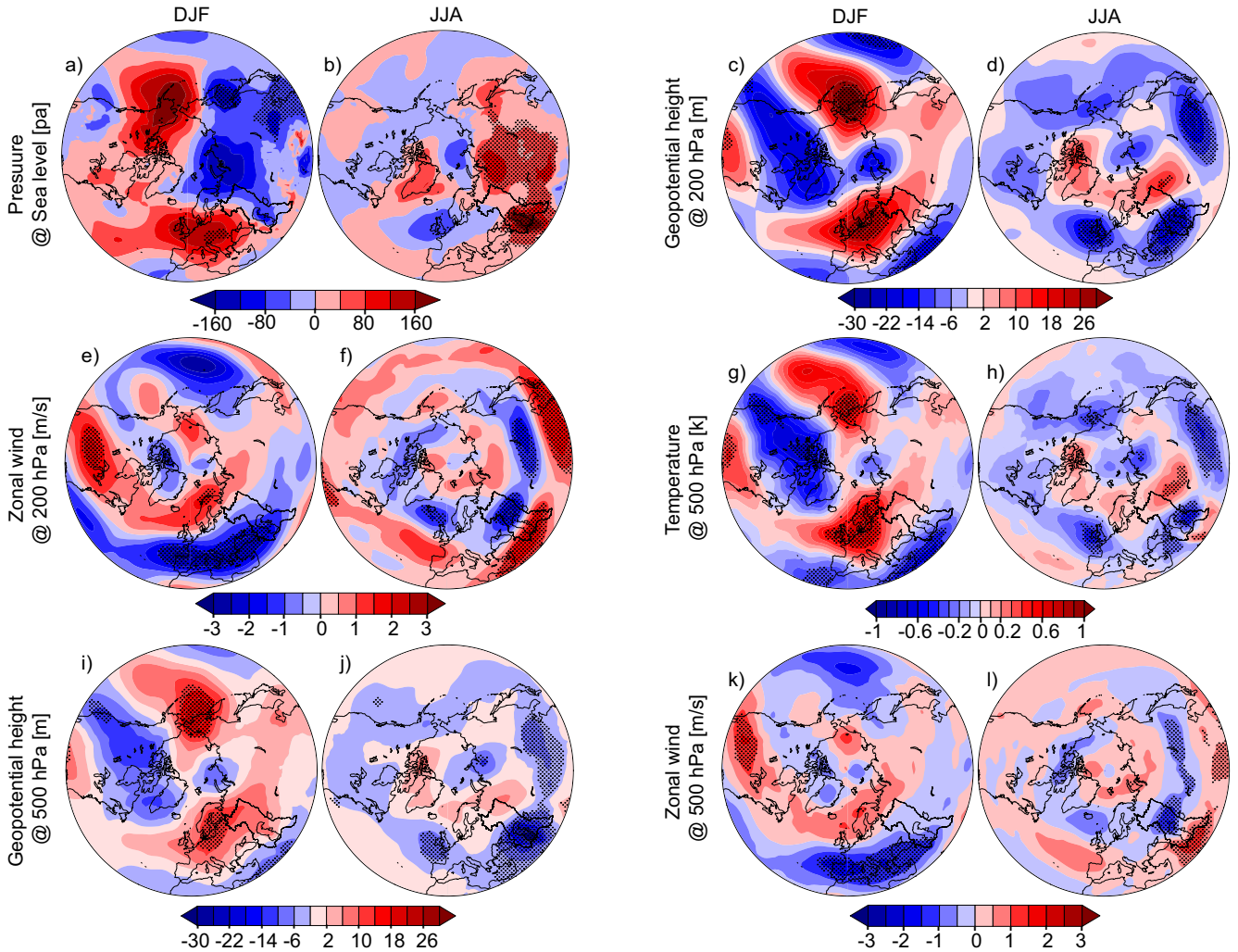

Figure 8. Winter and summer changes of sea level pressure (a and b), geopotential height at 200 hPa (c and d), zonal winds at 200 hPa showing changes in the jet stream (e and f), temperature at 500 hPa (g and h), geopotential height at 500 hPa (i and j), and zonal winds at 500 hPa (k and l) for current CS minus no-CS scenario. Stippling indicates regions where the change is statistically significant at the 95% level based on a Student's t-test. Abbreviations as in Figure 2.

around the North Pacific (Okhotsk Sea, Figure 9). This region has a particularly robust trend in sea-ice retreat as CS area increases. The impact is primarily in the winter months (the area is not sea-ice covered in summer; see Figure S10). With reduced sea-ice extent during winter as CS area increases, the lower atmosphere is exposed to large upward sensible heat flux anomalies (not shown) from the relatively warm ocean, producing a positive feedback that amplifies the initial change. This highlights the importance of performing coupled ocean-atmosphere modeling in order to capture relevant feedbacks in the climate system. It also hints at potential implications that are pertinent for human activities around the Arctic if large changes in CS area occur in the future (Nandini-Weiss et al., 2020).

4. Discussion

The results seen in this study confirm that variations in the surface area of the CS affect the climate in the regional catchment area and large-scale circulation patterns in the northern hemisphere. We note that both precipitation and evaporation increase (decrease) with a larger (smaller) CS area, since a larger CS produces and contributes more moisture to the atmosphere in this region compared to a smaller (no) CS, particularly during late autumn–early winter, when cold, dry air masses pass over the relatively warm CS, given the high heat capacity of the lake. Our study also confirms that evaporation plays a significant role on CSL variability

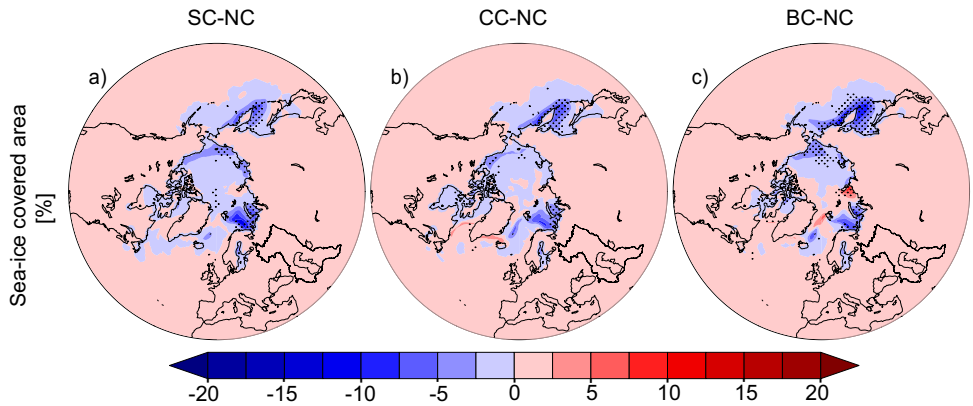

Figure 9. Annual mean changes in sea-ice covered area (%) for (a) small Caspian (SC), (b) current Caspian (CC) and (c) big Caspian (BC) with respect to no-Caspian (NC). Stippling indicates regions where the change is statistically significant at the 95% level, with significance levels estimated using a Student's t-test. NB: The version of Figures 5–9 that show only significant changes are included in the supplementary information (Figures S12–S16).

in a closed basin like CS. This is similar to findings by Chen et al. (2017), although their study did not include the compensating effect of precipitation when considering the impact of a warmer climate on CSL, and so they potentially overestimated a lowering of CSL due to warming. Enhanced precipitation in the south-west of the CS is clearly seen in our study. This contradicts a previous study by Arpe et al. (2019) possibly due to the lower horizontal resolution in their experiments and its influence on the representation of topography in that more mountainous area; but agrees with a regional climate modeling study by Nicholls and Toumi (2014) and a study by Tsuang et al. (2001).

The changes in precipitation during winter tend to follow evaporation. However, the changes are not linearly related throughout the year (similar to Nicholls & Toumi, 2014). Also, the magnitude of precipitation change is less than evaporation (~20% increase in precipitation over the CS catchment compared to ~50% increase in evaporation for large CS relative to no-CS). Our study shows evaporation and precipitation are lowered during spring by the presence of the CS (comparable to Lofgren, 1997; Nicholls & Toumi, 2014; Notaro et al., 2013). A partial explanation for this lies in the contrasting seasonal thermodynamics (and thermal inertia of the sea) and atmospheric moisture recycling. The summer atmospheric moisture recycling and distribution is known to play a key role in changing the regional climate (and convective instability). The amount of atmospheric moisture available is driven by the temperature difference between surface atmosphere and sea surface as well as surface easterly winds, and this relationship changes upon a given CS area. However, quantifying this relationship is quite complex and merits future investigation, as it is not within the scope of this study.

The change in precipitation and evaporation plays a vital role in the variability of the CSL as the area of the CS changes. The cumulative change in P-E is significant over the CS as the amount of evaporation exceeds precipitation for larger CS, but over the whole CS catchment area the change is not as significant. This has implications for the variability of CSL. The relationship between the CSL and P-E is complicated by the fact that changes in the CS area is not directly proportional to the change in CSL. A drop of CSL reduces the CS area and the total evaporation, which in turn affects the amount of water vapor in the atmosphere. Based on CSL offline simulations with THMB, we find significant CSL change when the CS area is very large or small compared to the current CS. In both cases, the runoff contribution from the CS catchment area and precipitation over the CS fail to balance evaporation over the sea, which results in either an increase or decrease in the CSL. More specifically, the resulting CSL in the THMB simulations is always closer to the present-day CSL than to the prescribed CSL in the corresponding CESM simulation for large and small CS. This points to a negative feedback between CS surface area (or CSL) and catchment-scale hydroclimate (i.e., water budget). Although precipitation in the south-western CS increases with increasing CSL (a positive feedback), the well-known negative lake surface-evaporation feedback still dominates. The feedbacks between the changes in CSL and the atmospheric water budget could be further examined and quantified by incorporating an interactive lake component with variable CS area within the climate model itself.

Sea-ice formation over the northern part of the CS plays a role in the surface heat and moisture budget. However, although sea-ice does form over the modeled CS (Figure S11), due to a warm bias in the region (as discussed in Nandini-Weiss et al., 2020) the model underestimates winter lake ice cover in the northernmost part of the CS under present-day conditions. Therefore, in the northern portion of the CS, heat fluxes from the lake surface into the atmosphere tend to be overestimated in winter. Under warmer climate conditions, when winter lake ice disappears (Tamura-Wicks et al., 2015), this model bias would also vanish. Hence, the importance of winter lake ice effects depends on the background climate.

Another key interest in this study is the impact of the changing CS areas on geographically remote regions in the northern hemisphere. The enhanced impact of surface air temperatures extending as far as east Siberia and north-west Pacific during the winter. These temperatures increase based on larger area changes and vice versa and are relative to a no-CS scenario. Enhanced warming over the north-western Pacific may be driven by changes in CS area dependent air masses. During winter, a larger CS area may lead to reduction in atmospheric stability due to CS being warmer than the surrounding air temperatures (also seen from Nicholls & Toumi, 2014). Hence, the seasonal temperature anomalies may lead to atmospheric instability (implications on cyclogenesis), during winter and greater stability (anti-cyclogenesis) during summer (Arpe et al., 2019; Nicholls & Toumi, 2014). The temperature changes are linked to sea level pressure changes, which show similar patterns for the same region, highlighting surface temperatures as drivers of low-level atmospheric circulation. Typically, enhanced (warmer) surface temperatures initiate updrafts, with resultant effects on lowering sea level pressure. Moreover, the winter season around the CS catchment area (relative to no-CS scenario) is dominated by lower pressure, stronger low-level winds, and increased moisture (enhanced temperature and evaporation changes).

A second relationship of interest focuses on the enhanced impact of precipitation in the central Asia region during summer. This increase (as CS increases) in precipitation may be driven by enhanced moisture supply to the atmosphere from the evaporative lake surface, but also by the associated changes seen previously for surface winds and westerly winds, which transport moisture afield. The westerlies are stronger in winter but weakened westerlies during summer may pick up moisture over the sea and transport it toward the eastern dry plains near central Asia. Also, the generally westerly flow in winds is disturbed by the Caucasus Mountains and restricted by the Elburz Mountains in the south. During the summer, associated reduced surface temperatures and weaker westerlies are seen relative to the no-CS scenario. Given this, it is particularly interesting that the summer precipitation increases as the CS area increases.

A third key relationship focuses on the enhanced impact of temperature on tropospheric geopotential height and zonal winds resulting in a shift in the location of the jet stream, which influences circulation patterns. Here we discuss two aspects. First, our results confirm the weakening of the 500 hPa troughs (geopotential height) over the northern Pacific with increasing CS area and vice versa. In the northern hemisphere, two frontal zones are well developed at the 500 hPa level, corresponding to strong thermal gradients. Heat sources can trigger stationary Rossby waves (Hoskins & Karoly, 1981) and a thermal response (changes in the temperatures at 500 hPa) may be the source for the wave pattern trigger seen for the geopotential height at 500 hPa. The second aspect relates to the southward shift in the location of the jet stream during summer. Different CS surface area sizes influence the atmospheric circulation patterns high in the troposphere (up to 500 and 200 hPa). Surface temperatures affect the geopotential height field in the upper atmosphere, which further impacts the zonal wind field due to the thermal wind relationship. Here, we note that the presence of different CS areas affects the thermal gradient (under the geostrophic assumption), which drives the jet stream speed and location (also seen in Lofgren, 1997 and Nicholls & Toumi, 2014). This summer relationship, where a surface thermal response triggers the reduction in geopotential height resulting in an enhanced dipole pattern in zonal wind anomaly at 200 hPa, was seen in the regional modeling study by Nicholls and Toumi (2014). However, we have also tested this summer relationship at the 500 hPa level and confirm that the summer temperatures at 500 hPa indeed influence the reduction in geopotential height, which results in the same (but weaker) dipole pattern of the zonal wind anomaly seen previously at the 200 hPa level. It is also comparable with findings for the Great Lakes region (Lofgren, 1997), where a stronger meridional temperature gradient (intensified in the north and weakened in the south) leads to a poleward shift in the winter jet stream. This study agrees with the study of Nicholls and Toumi (2014), but

here we expand on the understanding and inclusion of different realistic CS areas, using a state-of-the art high-resolution coupled global climate model.

The large-scale impact of the CS surface area, demonstrated in this study, has implications for global modeling of past and future climates. Paleoclimate simulations usually ignore changes in the CS surface area in their boundary conditions. In such studies, either a present-day CS surface area is assumed or the CS surface area changes according to changes in the global sea level (a pragmatic but unrealistic approach since changes in the CSL are independent of changes in the global sea level). Sometimes, paleoclimate modellers also simply remove the CS from the boundary conditions. Since the CS surface area has changed dramatically during Earth's history (Yanina, 2014), the wrong implementation of the CS in paleoclimate simulations may introduce additional biases, in particular in the CS catchment region, central Asia and the northern Pacific. The same holds for simulations of future climate change, since large changes of the CS water budget and, hence, CSL and CS surface area have been projected. A recent study by Nandini-Weiss et al. (2020) suggested a CSL decrease of 9 m (18 m) by the end of the 21st century for the RCP4.5 (RCP8.5) scenario.

By performing idealized simulations of four CS area changes, our findings aid in recognizing regional and large-scale climate impacts of the CS and strongly support the inclusion of more realistic CS area representation in future climate model developments. However, results shown here are from only one climate model and further multi-model studies could give different insights and possibly strengthen our findings. In the default version of the CESM a prescribed CS area is used, in common with all other similar climate models. This affects realistic CS moisture transports, which affects the atmospheric water budget, and reduces the potential for feedbacks between the climate and CSL. Furthermore, the circulation patterns of the Caspian Sea itself have not been considered in this study. However, the Caspian Sea has three zones of circulation due to the slightly saline water, the shape of the lake (bathymetry and elongated surface area in the north-south direction) and locations of riverine input (Dyakonov & Ibrayev, 2019; Leroy et al., 2020). Circulation in the sea is both wind-driven and thermohaline (density-driven) in nature. Potential future climate changes that may impact the distribution of the heat structure and the salinity regime may have implications for the variability of the sea surface temperature and evaporation rate over the sea (Diansky et al., 2018; Jamshidi, 2017; Komijani et al., 2019). However, such processes require high spatiotemporal resolutions which would be prohibitively expensive computationally to set-up. However, information from such a high resolution regional modeling scheme or observations could be used to parameterize simpler lake models or to prescribe lake fields in global models.

This sensitivity experiment is based on pre-industrial boundary conditions, as this is a benchmark (standard) for most climate modeling runs. We did not undertake the model experiments under palaeoclimate conditions but there may be interactions between changes to CS area and other palaeo-boundary condition changes for palaeoclimate time periods, and the importance of these will ultimately depend on the time slice being considered. For example, in the early Holocene, there was a severe lowstand in the CS, called the Mangyshlak regression. At this point climatic differences from the pre-industrial due to other boundary conditions were relatively small so we might expect that impact of the CS reduction in surface area would be relatively large. However, at the Last Glacial Maximum (LGM) the climate anomalies due to ice sheets and lower CO_2 are large and so we might expect that the impact of the CS highstand at this time would likely be relatively smaller than the other boundary conditions. However atmospheric circulation patterns would also be very different due to the presence of Eurasian icesheets, and so further model experiments exploring the impacts of these individual and combined boundary conditions would be needed to provide more insight.

5. Conclusions

Our choice of four CS sizes that have not been used in previous studies allows us identifying further impacts on regional climate over the CS catchment area as well as large-scale climate over the entire northern hemisphere. When compared to a no-CS scenario, evaporation over the sea increases with increasing area, while precipitation increases over the south-west CS with increasing area. While the latter process represents an interesting positive feedback on CS surface area, the well-known negative lake surface-evaporation feedback still dominates overall. The presence of the CS when compared with no-CS leads to enhanced

precipitation over central Asia and increased warming over the north-western Pacific during winter involving significant changes in sea ice. Also, our results demonstrate a weakening of the 500 hPa troughs over the northern Pacific with larger CS area. Lastly, we confirm a summer relationship of thermal response triggering mid and upper tropospheric geopotential height anomalies which results in a southward shift in the jet stream.

Our results indicate that an accurate representation of the CS in climate models is important to avoid additional biases when evaluating the climate processes over the CS catchment, central Asia, and the northern Pacific. This study allows for an accurate estimate of the change of the CSL from the change of the CS surface area when compared to a simulation carried out with an inaccurate CS area. Evidence from the palaeorecord demonstrates that the CSL has varied by >100 m over the Quaternary, with large attendant variations in CS area. Our study indicates that consideration of potential changes in CS area is likely important when modeling palaeoclimate scenarios, as well as for 21st century projections, but has so far not been given significant attention by the modeling community. Therefore, Coupling between modeled atmosphere and lake area variation within Global Circulation Models would be a significant advance to enable incorporation of the two-way feedbacks.

Conflict of Interest

The authors declare no conflicts of interest relevant to this study.

Data Availability Statement

For all of the described experiments, the climate variables used in this study are available as netcdf-file at PANGAEA (https://doi.pangaea.de/10.1594/PANGAEA.923110 or at https://www.pangaea.de/tok/45b656b49a02bcf1fe5dc934d596fe4766a3bb82).

Acknowledgments
This project has received funding from the European Union's Horizon 2020 research and innovation programme under the Marie Sklodowska-Curie Grant Agreement No. 642973; and the U.K.'s Natural Environment Research Council (NERC). The Evolution of Global Flood Risk (EVOFLOOD) Project Grant NE/S015590/1. All CESM simulations were performed on the supercomputer of the Norddeutscher Verbund fur Hoch-und Hochstleistungrechnen (HLRN3).

References

Amante, C., & Eakins, B. W. (2009). *Etopo1 1 arc-minute global relief model: Procedures, data sources and analysis. NOAA technical memorandum NESDIS NGDC-24*: National Geophysical Data Center.

Arpe, K., & Leroy, S. A. G. (2007). The Caspian Sea level forced by the atmospheric circulation, as observed and modelled. *Quaternary International*, *173–174*, 144–152. https://doi.org/10.1016/j.quaint.2007.03.008

Arpe, K., Molavi-Arabshahi, M., & Leroy, S. A. G. (2020). Wind variability over the Caspian Sea, its impact on Caspian Sea water level and link with ENSO. *International Journal of Climatology*, *40*, 6039–6054. https://doi.org/10.1002/joc.6564

Arpe, K., Tsuang, B. J., Tseng, Y. H., Liu, X. Y., & Leroy, S. A. G. (2019). Quantification of climatic feedbacks on the Caspian Sea level variability and impacts from the Caspian Sea on the large-scale atmospheric circulation. *Theoretical and Applied Climatology*, *136*(1–2), 475–488. https://doi.org/10.1007/s00704-018-2481-x

Arslanov, K. A., Yanina, T. A., Chepalyga, A. L., Svitoch, A. A., Makshaev, R. R., Maksimov, F. E., et al. (2016). On the age of the Khvalynian deposits of the Caspian Sea coasts according to 14°C and 230Th/234U methods. *Quaternary International*, *409*, 81–87. https://doi.org/10.1016/j.quaint.2015.05.067

Bezrodnykh, Y., Yanina, T., Sorokin, V., & Romanyuk, B. (2020). The northern Caspian Sea: Consequences of climate change for level fluctuations during the Holocene. *Quaternary International*, *540*, 68–77. https://doi.org/10.1016/j.quaint.2019.01.041

Broström, A., Coe, M., Harrison, S. P., Gallimore, R., Kutzbach, J. E., Foley, J., et al. (1998). Land surface feedbacks and palaeomonsoons in northern Africa. *Geophysical Research Letters*, *25*(19), 3615–3618. https://doi.org/10.1029/98GL02804

Chen, D., & Chen, H. W. (2013). Using the Köppen classification to quantify climate variation and change: An example for 1901–2010. *Environmental Development*, *6*(1), 69–79. https://doi.org/10.1016/j.envdev.2013.03.007

Chen, J. L., Pekker, T., Wilson, C. R., Tapley, B. D., Kostianoy, A. G., Cretaux, J. F., & Safarov, E. S. (2017). Long-term Caspian Sea level change. *Geophysical Research Letters*, *44*(13), 6993–7001. https://doi.org/10.1002/2017GL073958

Coe, M. T. (1998). A linked global model of terrestrial hydrologic processes: Simulation of modern rivers, lakes, and wetlands. *Journal of Geophysical Research*, *103*(D8), 8885–8899. https://doi.org/10.1029/98JD00347

Coe, M. T. (2000). Modeling terrestrial hydrological systems at the continental scale: Testing the accuracy of an atmospheric GCM. *Journal of Climate*, *13*(4), 686–704. https://doi.org/10.1175/1520-0442(2000)013<0686:MTHSAT>2.0.CO;2

Coe, M. T., & Bonan, G. B. (1997). Feedbacks between climate and surface water in northern Africa during the middle Holocene. *Journal of Geophysical Research*, *102*(10), 11087–11101. https://doi.org/10.1029/97jd00343

Contoux, C., Jost, A., Ramstein, G., Sepulchre, P., Krinner, G., & Schuster, M. (2013). Megalake chad impact on climate and vegetation during the late Pliocene and the mid-Holocene. *Climate of the Past*, *9*(4), 1417–1430. https://doi.org/10.5194/cp-9-1417-2013

Diansky, N. A., Fomin, V. V., Vyruchalkina, T. Y., & Gusev, A. V. (2018). Numerical simulation of the Caspian sea circulation using the marine and atmospheric research system. *Water resources*, *45*(5), 706–718https://doi.org/10.1134/S0097807818050056

Dyakonov, G. S., & Ibrayev, R. A. (2019). Long-term evolution of Caspian Sea thermohaline properties reconstructed in an eddy-resolving ocean general circulation model. *Ocean Science*, *15*, 527–541. https://doi.org/10.5194/os-15-527-2019

Forte, A. M., & Cowgill, E. (2013). Late Cenozoic base-level variations of the Caspian Sea: A review of its history and proposed driving mechanisms. *Palaeogeography, Palaeoclimatology, Palaeoecology*, *386*, 392–407. https://doi.org/10.1016/j.palaeo.2013.05.035

Hoskins, B. J., & Karoly, D. J. (1981). The steady linear response of a spherical atmosphere to thermal and orographic forcing. *Journal of the Atmospheric Sciences*, *38*(6), 1179–1196. https://doi.org/10.1175/1520-0469(1981)038<1179:TSLROA>2.0.CO;2

Hurrell, J. W., Holland, M. M., Gent, P. R., Ghan, S., Kay, J. E., Kushner, P. J., et al. (2013). The community earth system model: A framework for collaborative research. *Bulletin of the American Meteorological Society*, *94*(9), 1339–1360. https://doi.org/10.1175/BAMS-D-12-00121.1

Jamshidi, S. (2017). Assessment of thermal stratification, stability and characteristics of deep water zone of the southern Caspian Sea. *Journal of Ocean Engineering and Science*, *2*(3), 203–216.

Kakroodi, A. A., Kroonenberg, S. B., Goorabi, A., & Yamani, M. (2014). Shoreline response to rapid 20th century sea-level change along the Iranian Caspian coast. *Journal of Coastal Research*, *30*(6), 1243–1250. https://doi.org/10.2112/JCOASTRES-D-12-00173.1

Kakroodi, A. A., Leroy, S. A. G., Kroonenberg, S. B., Lahijani, H. A. K., Alimohammadian, H., Boomer, I., & Goorabi, A. (2015). Late Pleistocene and Holocene sea-level change and coastal paleoenvironment evolution along the Iranian Caspian shore. *Marine Geology*, *361*, 111–125. https://doi.org/10.1016/j.margeo.2014.12.007

Kislov, A. V., Panin, A. V., & Toropov, P. A. (2014). Present-day variations and paleodynamics of the Caspian Sea level as a standard for climate modeling data verification. *Russian Meteorology and Hydrology*, *39*(5), 328–334. https://doi.org/10.3103/S1068373914050069

Komijani, F., Chegini, V., & Siadatmousavi, S. M. (2019). Seasonal variability of circulation and air-sea interaction in the Caspian Sea based on a high resolution circulation model. *Journal of Great Lakes Research*, *45*(6), 1113–1129. https://doi.org/10.1016/j.jglr.2019.09.026

Koriche, S. A., Singarayer, J. S., & Cloke, H. L. (2021). The fate of the Caspian Sea under projected climate change and water extraction during the 21st century. *Environmental Research Letters*, *16*(9), 094024. https://doi.org/10.1088/1748-9326/ac1af5

Krijgsman, W., Tesakov, A., Yanina, T., Lazarev, S., Danukalova, G., Van Baak, C. G. C., et al. (2019). Quaternary time scales for the Pontocaspian domain: Interbasinal connectivity and faunal evolution. *Earth-Science Reviews*, *188*, 1–40. https://doi.org/10.1016/j.earscirev.2018.10.013

Kroonenberg, S. B., Kasimov, N. S., & Lychagin, M. Y. (2008). The Caspian Sea, a natural laboratory for sea-level change. *Geography, Environment, Sustainability*, *1*(1), 22–37.

Leroy, S. A. G., Lahijani, H. A. K., Crétaux, J.-F., Aladin, N. V., & Plotnikov, I. S. (2020). Past and current changes in the largest lake of the world: The Caspian Sea. In S. Mischke (Ed.), *Large asian lakes in a changing world: Natural state and human impact* (pp. 65–107): Springer International Publishing. https://doi.org/10.1007/978-3-030-42254-7_3

Lodh, A. (2015). Impact of Caspian Sea drying on Indian monsoon precipitation and temperature as simulated by RegCM4 model. *Hydrology: Current Research*, *6*(217). https://doi.org/10.4172/2157-7587.1000217

Lofgren, B. M. (1997). Simulated effects of idealized Laurentian Great Lakes on regional and large-scale climate. *Journal of Climate*, *10*(11), 2847–2858. https://doi.org/10.1175/1520-0442(1997)010<2847:SEOILG>2.0.CO;2

Molavi-Arabshahi, M., Arpe, K., & Leroy, S. A. G. (2016). Precipitation and temperature of the southwest Caspian Sea region during the last 55 years: Their trends and teleconnections with large-scale atmospheric phenomena. *International Journal of Climatology*, *36*(5), 2156–2172. https://doi.org/10.1002/joc.4483

Naderi-Beni, A., Lahijani, H., Mousavi Harami, R., Arpe, K., Leroy, S. A. G., Marriner, N., et al. (2013). Caspian Sea-level changes during the last millennium: Historical and geological evidence from the south Caspian Sea, *Climate of the Past*, *9*, 1645–1665. https://doi.org/10.5194/cp-9-1645-2013

Nandini-Weiss, S. D., Prange, M., Arpe, K., Merkel, U., & Schulz, M. (2020). Past and future impact of the winter North Atlantic Oscillation in the Caspian Sea catchment area. *International Journal of Climatology*, *40*(5), 2717–2731. https://doi.org/10.1002/joc.6362

Nicholls, J. F., & Toumi, R. (2014). On the lake effects of the Caspian Sea. *Quarterly Journal of the Royal Meteorological Society*, *140*(681), 1399–1408. https://doi.org/10.1002/qj.2222

Notaro, M., Holman, K., Zarrin, A., Fluck, E., Vavrus, S., & Bennington, V. (2013). Influence of the Laurentian Great Lakes on regional climate. *Journal of Climate*, *26*(3), 789–804. https://doi.org/10.1175/JCLI-D-12-00140.1

Peixoto, J. P., & Oort, A. H. (1992). *Physics of climate*: American Institute of Physics.

Rodionov, S. N. (1994). *Global and regional climate interaction: The Caspian Sea experience*: Springer Science+Business Media, B.V.

Sousa, P. M., Ramos, A. M., Raible, C. C., Messmer, M., Tomé, R., Pinto, J. G., & Trigo, R. M. (2020). North Atlantic integrated water vapor transport—From 850 to 2100 CE: Impacts on western European rainfall. *Journal of Climate*, *33*(1), 263–279. https://doi.org/10.1175/JCLI-D-19-0348.1

Sousounis, P. J., & Fritsch, J. M. (1994). Lake-aggregate mesoscale disturbances. Part II: A case study of the effects on regional and synoptic-scale weather systems. *Bulletin - American Meteorological Society*, *75*(10), 1793–1811. https://doi.org/10.1175/1520-0477(1994)075<1793:LAMDPI>2.0.CO;2

Tamura-Wicks, H., Toumi, R., & Budgell, W. P. (2015). Sensitivity of Caspian Sea-ice to air temperature. *Quarterly Journal of the Royal Meteorological Society*, *141*, 3088–3096. https://doi.org/10.1002/qj.2592

Tsuang, B. J., Tu, C. Y., & Arpe, K. (2001). *Lake parameterization for climate models* (p. 316). Max Planck Institute for Meteorology.

Valiantzas, J. D. (2006). Simplified versions for the penman evaporation equation using routine weather data. *Journal of Hydrology*, *331*(3), 690–702. https://doi.org/10.1016/j.jhydrol.2006.06.012

Yanina, T., Bolikhovskaya, N., Sorokin, V., Romanyuk, B., Berdnikova, A., & Tkach, N. (2020). Paleogeography of the Atelian regression in the Caspian Sea (based on drilling data). *Quaternary International*. https://doi.org/10.1016/j.quaint.2020.07.023

Yanina, T. A. (2014). The Ponto-caspian region: Environmental consequences of climate change during the late Pleistocene. *Quaternary International*, *345*, 88–99. https://doi.org/10.1016/j.quaint.2014.01.045